DYNA
ISSN: 0012-7353
Universidad Nacional de Colombia

Paredes-Madrid, Leonel; Matute, Arnaldo; Cruz-Pacheco,
Andrés F.; Parra-Vargas, Carlos A.; Gutiérrez-Velásquez, Elkin I.
Experimental characterization, modeling and compensation of hysteresis in force sensing resistors
DYNA, vol. 85, no. 205, 2018, April-June, pp. 191-198
Universidad Nacional de Colombia

DOI: https://doi.org/10.15446/dyna.v85n205.66432

Available in: https://www.redalyc.org/articulo.oa?id=49657889025

- How to cite
- Complete issue
- More information about this article
- Journal's webpage in redalyc.org

Scientific Information System Redalyc
Network of Scientific Journals from Latin America and the Caribbean, Spain and Portugal
Project academic non-profit, developed under the open access initiative

UNIVERSIDAD NACIONAL DE COLOMBIA
SEDE MEDELLÍN
FACULTAD DE MINAS

DYNA
http://dyna.medellin.unal.edu.co/

Experimental characterization, modeling and compensation of hysteresis in force sensing resistors

Leonel Paredes-Madrid [a] Arnaldo Matute [a], Andrés F. Cruz-Pacheco [b], Carlos A. Parra-Vargas [b] & Elkin I. Gutiérrez-Velásquez [a]

[a] *Facultad de Ingeniería Mecánica, Electrónica y Biomédica Universidad Antonio Nariño, Tunja, Colombia. paredes.leonel@uan.edu.co, arnaldo.matute@uan.edu.co, elkin.gutierrez@uan.edu.co*
[b] *Grupo de Física de Materiales (GFM), Universidad Pedagógica y Tecnológica de Colombia, Tunja, Colombia. andresfelipe.cruz@uptc.edu.co, carlos.parra@uptc.edu.co*

Received: July 18th, 2017. Received in revised form: April 11th, 2018. Accepted: May 5th, 2018.

Abstract
Force Sensing Resistors (FSRs) exhibit considerable amounts of hysteresis and repeatability error inhibiting their usage in applications that require high-accurate force readings. This paper presents the hysteresis characterization and modeling of the Tekscan A201-1 FSR employing the Preisach Operator (PO) function. In order to compensate for hysteresis during sensor operation, the inverse PO was numerically found on the basis of the Closest Match Algorithm (CMA). A test bench, capable of handling sixteen sensors simultaneously, was built, which allowed the characterization and later testing of the CMA. Grip force profiles were applied to the sensors during testing and the experimental results showed a considerable reduction in the force estimation error compared with the linear regression method proposed by the manufacturer. These results enable a wider use of FSRs in applications with tight accuracy requirements. Finally, a generalized sensor model for hysteresis compensation that simplifies the obtaining of PO parameters is presented.

Keywords: hysteresis; force sensing resistors; Preisach operator; closest match algorithm.

Caracterización experimental, modelado y compensación de la histéresis en sensores de fuerza resistivos

Resumen
Los Sensores de Fuerza Resistivos (FSRs) despliegan cantidades considerables de histéresis y de error de repetitividad que inhiben su uso en aplicaciones que requieren lecturas de fuerza de alta precisión. En este trabajo se presenta la caracterización y modelado de histéresis del sensor de presión Tekscan A201-1 empleando la función Operador de Preisach (OP). Con el fin de compensar la histéresis durante el funcionamiento del sensor, el OP inverso se halló numéricamente sobre la base del algoritmo de coincidencia más cercana (CMA). Se construyó un banco de pruebas, capaz de manejar dieciséis sensores simultáneamente, lo que permitió la caracterización y posterior prueba del CMA. Los perfiles de fuerza de agarre se aplicaron a los sensores durante la prueba y los resultados experimentales mostraron una reducción considerable del error de estimación de la fuerza en comparación con el método de regresión lineal propuesto por el fabricante. Estos resultados abren el camino para un uso más amplio de los FSRs en aplicaciones con exigentes requisitos de precisión. Finalmente, un modelo de sensor generalizado para compensación de histéresis que simplifica la obtención de los parámetros PO, es presentado.

Palabras clave: sensores de fuerza resistivos; operador de Preisach; algoritmo de coincidencia más cercana.

1. Introduction

Biomechanical researches strongly rely on accurate force measurements to provide reliable studies and outstanding developments: ground reaction forces occurring during gait analysis and gripping forces occurring during object manipulation are only some applications that demand non-invasive and accurate force measurements.

How to cite: Paredes-Madrid, L., Matute, A., Cruz-Pacheco, A.F., Parra-Vargas. C.A. and Gutiérrez-Velásquez, E.I., Experimental characterization, modeling and compensation of hysteresis in force sensing resistors. DYNA, 85(205), pp. 191-198, June, 2018.

© The author; licensee Universidad Nacional de Colombia.

Inertia and position readings are also demanded in biomechanical studies; with the added complexity that the employed transducers must be installed with minimal interference on the human or animal under study in order to avoid discomfort during motion, consequently, the sensors in Biomechanical studies must be either low profile or such variables must be remotely tracked when possible [1,2].

Performing accurate position and inertia readings has been practically resolved through the usage of encoders, resolvers and Inertial Measuring Units (*IMUs*). However, if such sensors result too bulky, high-speed cameras can be used instead [3]. However, performing accurate force readings has always been a difficult task in biomechanical studies because force, unlike position, cannot be remotely tracked.

Force Sensing Resistors (*FSRs*) are cost-affordable force sensors that can be easily integrated into multiple Biomechanical applications [4-6]. Nonetheless, the main reasons for its widespread usage are their low profile and low weight, which are highly desirable characteristics when attempting to perform non-invasive force measurements [6]. Another reason for their wide acceptance is the simple interface circuit required to read sensor's output, e.g.: voltage dividers or inverting amplifiers. When using an inverting amplifier, see Fig. 1a, an estimation of sensor's conductance ($1/R_s$) is obtained through output voltage (V_{o1}). Conversely, when using a voltage divider, see Fig. 1b, sensor's resistance (R_s) is measured through V_{o2}.

Commercially available *FSRs* can be found on different shapes and nominal ranges: round (FSR400 and FSR402) and squared (FSR406 and FSR408) *FSRs* are manufactured by Interlink Electronics, Camarillo, CA [7]. Tekscan Inc. from South Boston, MA, offers round (A201-1, A201-25 and A201-100) and several customizable *FSRs* in his product catalog [8], see Fig. 1c and Fig. 1d. Unfortunately, the overall performance of *FSRs* is poor compared to well-established force sensing solutions such as load cells and strain gauges. Previous works from Lebosse [9], Hollinger [10] and Komi [11] present a comprehensive review on *FSR* limitations. Hysteresis and drift are typically one or two orders of magnitude greater in *FSR*s than in load cells. These conditions are the main drawbacks for the extensive usage of *FSRs* in industrial and research applications, but a great effort is currently placed on improving their performance.

One trend, within *FSR* research, is to model sensors' response with the aim of compensating hysteresis and drift. Relevant works on this scope have been developed by Lebosse [9], Schofield [5], Dabling [12], Vecchi [13] and Urban [14]. Likewise, authors' previous work has demonstrated that the A201 sensors, working on the piezoresistive principle, are also capable of exhibiting a piezocapacitive response. Different methods were proposed and evaluated by the authors to combine Capacitance (C_s) and Conductance (V_{o1}) readings with the aim of increasing *FSR* accuracy under static loading [15, 16]. It must be noted that DC/AC voltages were alternately applied to the *FSRs* to read V_{o1} and C_s respectively, followed by a feedforward neural network to optimally combine V_{o1} and C_s readings. When compared to the purely conductance model of Fig. 1e [8], a 64% reduction in the force Mean Squared Error (*MSE*) was obtained. The reduction in the *MSE* was done at the price of increasing the complexity of the driving circuit which may result prohibitive for certain applications with power or space constraints.

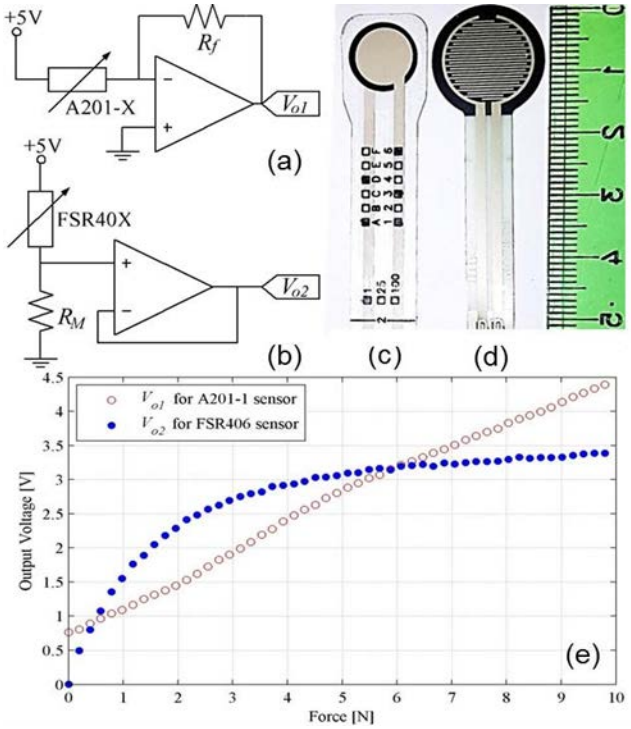

Figure 1. Driving circuits for: (a) FlexiForce A201-X, (b) Interlink FSR40X. Pictures of: (c) A201-1 and (d) FSR402 next to a ruler in centimeters. (e) Typical sensors' response: A201-1 (circle red) and FSR406 (solid blue). Source: The authors.

By modeling *FSR's* hysteresis through the Preisach operator [17], an improved algorithm for estimating applied forces is here presented. The algorithm only requires conductance readings form the sensor, and thus, the simple driving circuit of Fig. 1a is needed, or Fig. 1b when using Interlink sensors. A considerably computational effort is required to run the inverse Preisach algorithm, but such an effort is justified when the force *MSE* is dramatically reduced. In order to obtain a valid generalization of results, a total of sixteen A201-1 FlexiForce sensors are used; this sensor matches the required force range (*4.5N*) of biomechanical applications involving grip and grasp operations. Nonetheless, the methods henceforth discussed are applicable to other models of *FSRs*.

This paper is organized as follows: Section II describes the experimental setup for gathering sensor data. Later in Section III, experimental data from the sixteen A201-1 sensors are presented with statistics regarding hysteresis. A brief description of the Preisach Operator and its inverse are also available on Section III. Later in Section IV, grip force profiles are exerted on the A201-1 sensors and the inverse Preisach algorithm is tested and compared with the traditional conductance model. In Section V, a generalized sensor model based on the Preisach Operator is presented, followed by conclusions and future work on Section VI.

2. Experimental Set-Up

Previous work demonstrated that the A201-X sensors can be electrically modeled as a parallel R_s-C_s device as shown in Fig. 2a [15,16], with R_s exhibiting a hyperbolical dependence on the applied force (F). Since this paper focusses on reducing the force *MSE* through conductance readings only, capacitance measurements are not henceforth considered. For linearization purposes, conductance variations – measured through V_{o1} – have been preferably used in several studies to estimate F [8, 9, 12, 15]; this is possible by inverting the model of Fig. 1e, which yields:

$$F = mV_o + b \tag{1}$$

Where m and b are obtained from a least-squares minimization process; the whole procedure is known in literature as sensor characterization and may comprise only increasing or increasing/decreasing forces. It must be noted that the application of either pattern produces a significant effect in m and b values given the hysteresis in the device; this is later exemplified on Section IV. The test bench for sensor characterization and testing comprises electrical and mechanical sensors/actuators as described next.

2.1. Mechanical setup

In order to get a trade-off between nominal force and resolution, a linear stepper motor was accommodated with a spring to exert forces over the bunch of sensors depicted in Fig. 2b. The mechanical compliance of the test bench was modified through the stiff constant of the spring; and the force control loop was closed using data from a high accuracy LCHD-5 load cell with 22N capacity. The set-up could arrange up to sixteen sensors simultaneously with a resolution of 1.4mN and a maximum dF/dt of 22.6N/s. These characteristics were more than enough to emulate force profiles exerted during grip and grasp operations such as those reported by Stolt [18] and Melnyk [19].

The sensors were arranged in a sandwich configuration and then placed inside a temperature chamber that held operating temperature at 25ºC±1ºC to avoid undesired effects caused by thermal drift, see Fig 2c. Considering that the main scope of this article is to reduce the force *MSE* through hysteresis modeling and compensation, it was not embraced the inclusion of changing temperatures as an additional variable. Finally, it must be noted that the sandwich configuration depicted in Fig. 2b added extra weight to the sensors located at the bottom; this condition was taken into account for the linear regression method (1) and the Preisach Operator later described on Sections III, IV.

2.2. Electrical setup

A modified version of the circuit from Fig. 1a was implemented to perform voltage readings in the sixteen sensors, see Fig. 3. A time-multiplexed scheme comprising four analog multiplexers (ADG444) was implemented to readout V_o. The feedback Resistor (R_f) was set to 10KΩ and the supply Voltage (V_s) was set to -1V.

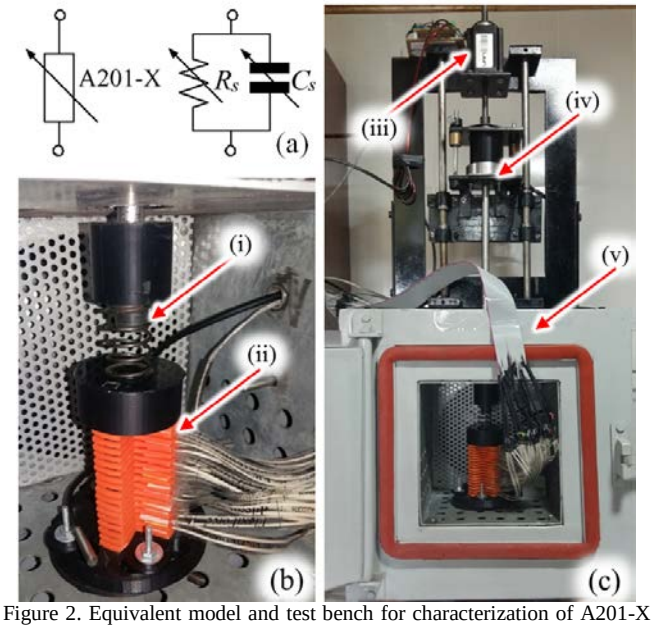

Figure 2. Equivalent model and test bench for characterization of A201-X sensors. (a) Black box model and equivalent circuit for an A201-X *FSR*. (b) Zoom-in picture depicting the spring (i) for mechanical compliance of the test bench and the bunch of sixteen A201-1 sensors (ii) arranged in a sandwich configuration. (c) Picture of the test bench showing the stepper motor (iii), the LCHD-5 load cell (iv) and the temperature chamber (v). Source: The authors.

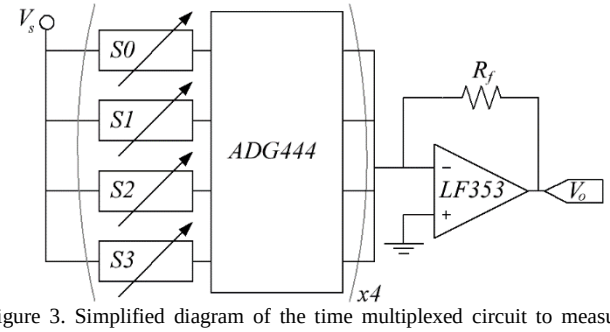

Figure 3. Simplified diagram of the time multiplexed circuit to measure conductance (V_o) in sixteen A201-1 sensors, S0 through S15. Source: The authors.

It must be remarked that the FlexiForce sensors exhibit a subtle saturation effect in the form of hyperbolic tangent in regard to V_s variations; this avoids that m and b can be recalculated when V_s is changed given that k in (2) changes from one sensor to another [16]. In practice, this implies that (1) is valid only for a constant V_s during sensor operation:

$$V_o = -(mF + b)\,atanh\,(V_s / k) \tag{2}$$

3. Hysteresis characterization, modeling and compensation based on the Preisach operator

3.1. Characterization of hysteresis in FSRs

Triangle force profiles of 4.5N were exerted over the sensors to observe V_o during loading and unloading events.

Equation (3) was employed to assess the Hysteresis Error (*HE*) based on the metrics shown on Fig. 4a. Results from the sixteen sensors are represented by data points on Fig. 4b.

$$HE = 100\% \cdot (V_o^u - V_o^l)/V_o^M \tag{3}$$

Note that hysteresis ranges from 7.6% to 17%, with the maximum V_o^u–V_o^l occurring typically at half of the nominal sensor range, such values notably differ from what the sensor manufacturer reports at [8] with *HE*<4.5%. However, the manufacturer estimates the *HE* at 80% of the nominal sensor range. Dabling reports in [12] a 7.4% hysteresis for the Tekscan A401-25 sensor, which is consistent with the results from Fig 4b.

3.2. Modeling hysteresis through the Preisach operator

In order to compensate for hysteresis, it needs first to be modeled. The Preisach Operator (*PO*) is a common approach to model hysteresis; it has been successfully employed in nanopositioning applications with piezoelectric and magnetostrictive actuators [17, 20]. An in-depth explanation of the *PO* theory has not been provided here, but readers may refer to Tan [21] and Visone [17] for such a purpose.

The ability of the Preisach Operator to model hysteresis is next described with an example focused on the A201-1 sensor, where $R_{\alpha,\beta}[F,H(t\text{-}1)]$ is the delayed relay output represented in Fig. 5a as *H* and as *H(t)* in (4). The applied force, *F*, is the time-varying input.

$$H(t) = R_{\alpha,\beta}[F, H(t-1)] = \begin{cases} 1 & for \;\; F \geq \alpha \\ H(t-1) & for \;\; \beta < F < \alpha \\ -1 & for \; F \leq \beta \end{cases} \tag{4}$$

The function $R_{\alpha,\beta}[F,H(t\text{-}1)]$ is known in literature as the Preisach Operator or Hysteron, where parameters α and β come from the discretization of *F* into n_h levels, summing a total of n_q Hysterons:

$$n_q = n_h(n_h+1)/2 \tag{5}$$

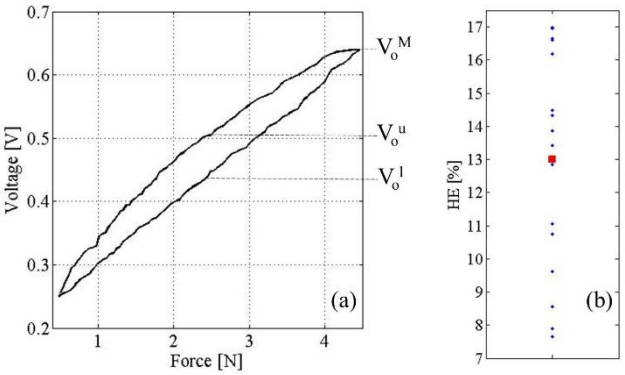

Figure 4. Hysteresis in the A201-1 sensor. (a) Plot representing the maximum voltage difference between loading (V_o^l) and unloading (V_o^u) events, occurring at the same *F*. (b) Scatter plot of the *HE* for sixteen A201-1 sensors. The average *HE* is shown with a squared red marker.
Source: The authors.

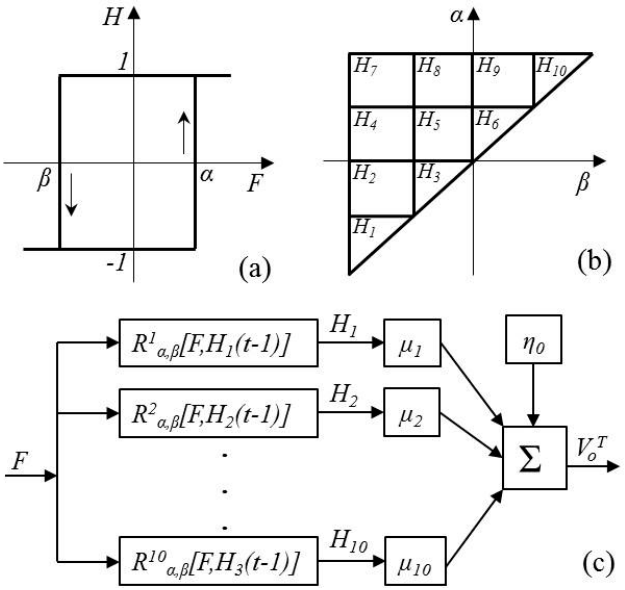

Figure 5. Preisach Operator and elements. (a) Plot of the delayed relay output representing the mathematical function of a Hysteron. (b) Preisach plane with n_h=*4* and 10 Hysterons. (c) Block diagram representing the totaling function for modeling hysteresis in the A201-1 FSR.
Source: The authors.

As in Fig. 5b with n_h=*4*, there is a total of 10 Hysterons (H_1~H_{10}). The totaling function ($V_o^T(t)$) is a discrete function that embraces the contribution from each delayed relay output (H_1~H_{10}) weighted by (μ_1~μ_{10}) plus an offset (η_0); this process is performed on each sampling interval to obtain a discrete model of the sensor hysteresis. A graphical representation of the totaling process is depicted on Fig. 5c.

At the beginning of a trial, all of the Hysterons are deactivated, i.e., initialized at *y(t-1)=-1*, see Fig. 6a; this implies that $F(t_1) \leq \alpha_1$. As $F(t_2)$ increases beyond α_3, Hysterons H_1 to H_6, are activated and their relay outputs change from *-1* to *1*. Active relay outputs are gray colored in Fig. 6a and ahead. Later, the applied force decreases up to $F(t_3)$ where $F(t_3) \leq \beta_2$, and thus, Hysterons H_3, H_5 and H_6 are deactivated as shown on Fig. 6c. Finally, in Fig. 6d, force is increased again up to $F(t_4)$ and the only Hysteron that changed is H_3 since $\alpha_2 < F(t_4) < \alpha_3$.

The ability of the Preisach Operator to model hysteresis is exemplified as follows: let's say that in a new trail represented in Fig. 6e, the applied force is straight incremented from $F(t_1) \leq \alpha_1$ up to $F(t_5)$, with $F(t_5)=F(t_4)$. Note that in Fig. 6e the Hysterons H_1 to H_3 are activated, which differs from the previous memory curve of Fig 6d. Such a difference yields different values on the output totaling function, $V_o^T(t)$, because of the different trajectories employed to reach $F(t_4)$ and $F(t_5)$ on each case.

The weight values of each Hysteron, μ_1~μ_{10}, and the offset, η_0, are estimated on an empirical basis, following a characterization process somewhat similar to that recommended by the sensor manufacturer [8]. In a general case with n_h levels of discretization, there is a total of n_q Hysterons that are grouped in the so-called memory curve (Ψ). The Preisach density function ($\mu_{(\alpha,\beta)}$) is defined as the collection of weights representing the contribution of each

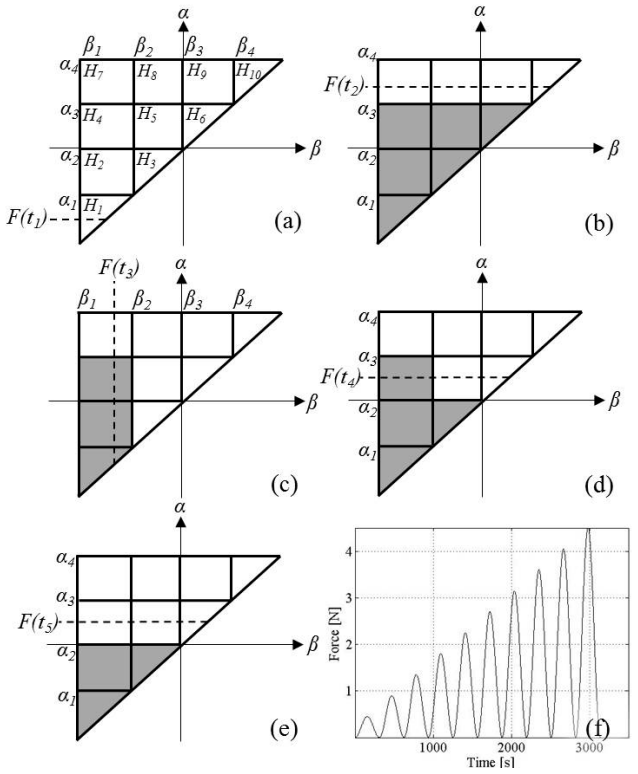

Figure 6. Preisach plane and input signal for hysteresis characterization, active hysterons are gray colored. (a through d) Evolution of the Preisach plane under increasing and decreasing forces with initial condition $\Psi_0=(H_1\sim H_{10})=-1$ at Fig. 6a. (e) Final Preisach plane for an input force $F(t_5)$ with initial condition $\Psi_0=(H_1\sim H_{10})=-1$.(f) General form of the required input signal for hysteresis characterization.
Source: The authors.

Hysteron to the totaling function, $V_o^T(t)$. The function $\mu_{(\alpha,\beta)}$ is nonnegative with a total of n_q elements. It must be noted that in order to model hysteresis, a total of n_q+1 parameters – $\mu_{(\alpha,\beta)}$ plus η_0 – must be estimated through a least-squares minimization process that ensures the nonnegative constraint of the Preisach density function. During characterization, it is important that the input force profile ensures the activation and deactivation of all the Hysterons; by doing this, an appropriate estimation of $\mu_{(\alpha,\beta)}$ and η_0 is obtained.

Stakvik presented in [20] a guideline for creating an adequate input signal intended for hysteresis characterization; the signal consists of incremental-amplitude sine waveforms as shown on Fig. 6f. It must be remarked that the hysteresis is a rate independent phenomenon, and thus, the frequency of the input-sine profile does not affect the identification process.

Finally, the identification of $\mu_{(\alpha,\beta)}$ and η_0 was carried out by applying a modified version of Fig. 6f. Triangle force profiles were used instead of sines with forty evenly spaced amplitudes starting from 0N up to 4.5N. Likewise, the discretization level was set to $n_h=40$ during the data fitting process that estimated $\mu_{(\alpha,\beta)}$ and η_0. The resulting $\mu_{(\alpha,\beta)}$ is plotted on Fig. 7 for one of the sixteen sensors previously shown on Fig. 2b, similar density functions were obtained for the rest of sensors.

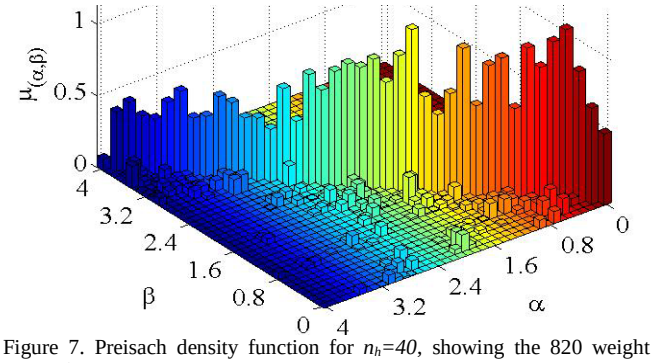

Figure 7. Preisach density function for $n_h=40$, showing the 820 weight values for an A201-1 FlexiForce sensor.
Source: The authors.

In practice, the maximum value of n_h is limited by the Repeatability Error (*RE*) of the device; typically *RE=2.5%* for the A201-1 sensor [8]. This implies that the uncertainty in sensor output, V_o, for a given applied force is of 2.5% and thus, the sensor can resolve a maximum of 100/2.5 force intervals without overlapping.

3.3. *Compensating hysteresis in FSRs through the inversion of the Preisach operator*

When estimating *F* based on V_o readings, the *PO* model must be inverted in order to compensate for hysteresis. Unfortunately, an analytical expression for the delayed relay operator cannot be formulated; and thus, an approximate numerical solution must be found instead.

Given the initial conditions: Ψ_0 curve with all Hysterons deactivated, $(H_1\sim H_{10})=-1$, and the applied force $F_0=0N$. At the next sampling interval with $F_1>F_0$, the numerical inversion algorithm activates the Hysterons following the same order depicted in Fig. 6, i.e. H_1, H_2-H_3, H_4-H_5-H_6, and so on. The process is repeated until $V_o^T(t)$ reaches the closest match to the measured voltage V_1 at the *FSR*. The required force to activate the above-cited Hysterons is the approximate numerical solution of the inverse *PO* model. The procedure is conveniently known in literature as the Closet Match Algorithm (*CMA*) [21]. The output of the *CMA* is discrete (*F*), just as the *PO* model is. However, a continuous implementation of the *CMA* has been already developed in [20], but for space constraints, it has not been discussed or implemented here.

4. Experimental results and analysis

Grip force profiles, based on grip data issued from Stolt [18] and Melnyk [19], were exerted on the A201-1 sensors using the experimental set-up previously described on Section II. The performance of the *CMA* to estimate *F* was comparatively evaluated with the linear regression model (1), which is the manufacturer recommended method. It must be noted that the linear regression model is the preferred method in research applications [4,5,9-13]. Two sets of *m* and *b* constants were calculated using the triangle force profiles of Section III.B. The first set of *m* and *b* constants used only the increasing data points, whereas the second fit employed the whole data.

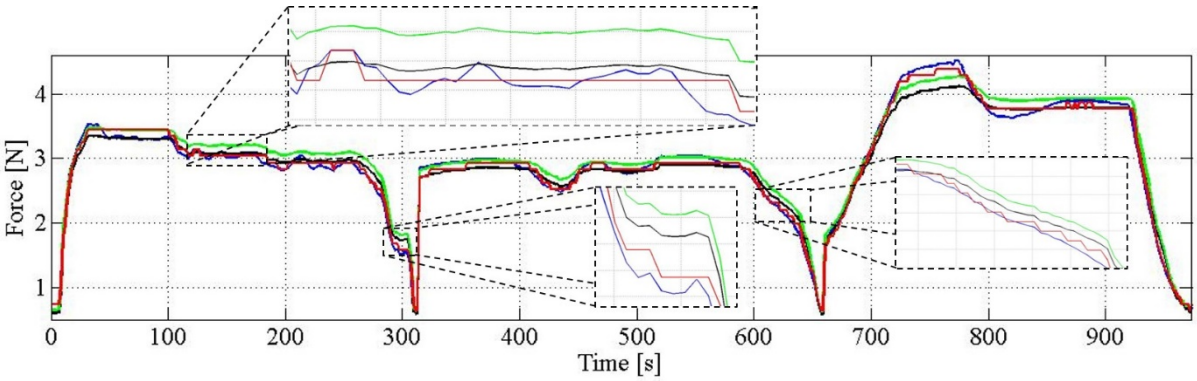

Figure 8. Force estimation through different methods: (red) *CMA* using a sensor-tuned Preisach density function and η_0, linear regressions using increasing data points only (green) and the entire dataset (black). Real force profile based on grip data from Stolt [18] and Melnyk [19] (blue).
Source: The authors.

Experimental results for a given sensor are graphed on Fig. 8, together with an error bar plot on Fig. 9 representing the force *MSE* for the sixteen sensors and the three models, i.e.: the *CMA* and the two aforesaid linear regressions. In average, the *CMA* yields a considerable reduction in the *MSE* compared to the models based on (1), 54% and 76% respectively. The reduction in the force *MSE* is paid by a larger computation time, which may limit the usability of the *CMA* in some real-time applications, but if time is not a constraint; the *CMA* can run off-line and get the best of a *FSR*. This is the case of most biomechanics researches in which data are collected and later analyzed [4, 5]. However, a fast implementation of the *CMA* is possible if dedicated hardware is used, i.e., employing FPGA technology [22].

Note that the dispersion of the *MSE* is narrowed when force estimation is done on the *CMA* (red bars on Fig. 9), this occurs because the remaining *MSE* is only produced by: the Repeatability Error, *RE*, and the quantization error derived from the discrete *CMA*. The contribution of the *HE* to the *MSE* is suppressed thanks to the *PO* modeling and compensation via the *CMA*. Further reduction of the *MSE* is possible if a continuous implementation of the *CMA* is performed, just as Stakvik demonstrated in [20]. This statement can be illustrated from the zoom-in plot at the top of Fig. 8. Note that both linear regressions exhibit a subtle swinging due to V_o variations, nonetheless, such variations are not great enough to change the memory curve Ψ, and consequently, the *CMA* yields a constant output. The implementation of a continuous *CMA* can better adapt to subtle V_o variations amid a constant memory curve Ψ, and thus, the force *MSE* would be further reduced.

5. Generalized sensor model for hysteresis compensation: an approach

Obtaining $\mu_{(\alpha,\beta)}$ and η_0 is not a straightforward procedure; specialized hardware is required and a time consuming characterization must be performed followed by non-trivial programing. Fortunately, it is possible to simplify the characterization process if the parametrization is performed as follows: Given b_0, the output voltage of a *FSR* at null force, and V_{nom}, the maximum output voltage at the nominal sensor range; then, the following linear transformation can be applied

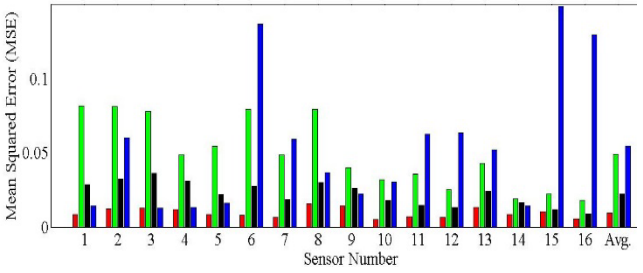

Figure 9. Error bar plot depicting the force *MSE* for the sixteen A201-1 sensors operating on the following estimation methods: (red) *CMA* using a sensor-tuned Preisach density function and η_0, linear regressions using increasing data points only (green) and the entire dataset (black), *CMA* using the Preisach-scaled parameters, $\mu^s_{(\alpha,\beta)}$ and η^s_0 (blue).
Source: The authors.

to any V_o reading during both: the estimation of $\mu_{(\alpha,\beta)}$ and η_0, and later, during sensor operation.

$$V_o{}^s = (V_o - b_0)/(V_{nom} - b_0) \tag{6}$$

The scaled output voltage (V_o^s) is normalized, just as the resulting Preisach-scaled parameters are, $\mu^s_{(\alpha,\beta)}$ and η^s_0; this implies that they can be used to estimate F with hysteresis compensation for any sensor, requiring only the experimental measuring of b_0 and V_{nom} on each new device.

However, it must be pointed out that during sensor operation, the *CMA* running on the basis of $\mu^s_{(\alpha,\beta)}$ and η^s_0 can compensate for a specific amount of *HE*, see Fig 4, this implies that if a given sensor exhibits a larger *HE* than that modeled by $\mu^s_{(\alpha,\beta)}$ and η^s_0, the resulting F will still exhibit some hysteresis (underfitting case). Conversely, if a given sensor has a lower *HE*, the resulting F will reflect hysteresis overfitting; both cases are presented on Fig. 10. Hysteresis overfitting is characterized by a time-ahead output during sensor unloading (green data on Fig. 10), especially noticeable around the maximum $V_o{}^u$–$V_o{}^l$ which occurs at half of the nominal sensor range, see Fig. 4. Conversely, if hysteresis is under-fitted, the *CMA* produces a lagged sensor output during the unloading stage (red line on Fig. 10).

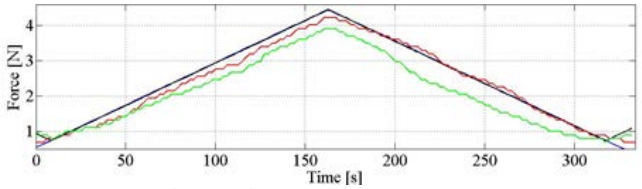

Figure 10. Triangle force profile (blue) and sensors output response showing hysteresis underfitting (red) and overfitting (green).
Source: The authors.

The Preisach-scaled parameters were obtained by applying the linear transformation (6) to the data gathered for the sixteen sensors. The resulting $\mu^s_{(\alpha,\beta)}$ and η^s_0 were later used to estimate *F* using the *CMA*. The blue error bars of Fig. 9 shows the resulting *MSE* when using the Preisach-scaled parameters during force estimation. Note that the *MSE* is higher than that reported on Section IV (individual Preisach parameters tuned for each sensor); this is a logical consequence of hysteresis-overfitting and underfitting. Likewise, mixed results were obtained when comparing to the linear regression methods, indicating that additional work is required on this subject.

6. Conclusion and future work

The Preisach Operator and the Closest Match Algorithm (*CMA*) have been successfully implemented on sixteen A201-1 sensors to both: model hysteresis and compensate for hysteresis effects during sensor operation. In the latter case, a considerably reduction of 54% was obtained in the force *MSE* compared with the manufacturer-recommended method based on linear regression. This is an important contribution that narrows the gap between the highly accurate load cells and the low-profile low-cost FSRs. Further *MSE* reduction is possible by implementing a continuous *CMA*, this is left as a pending task for future work. It must be remarked that hysteresis modeling and compensation required no-additional hardware during sensor operation, which is a highly desirable characteristic in applications with power or space constraints.

Considering that hysteresis modeling is not a straightforward procedure, a generalized model for hysteresis compensation has been proposed for the A201-1 sensor. However, mixed results were obtained because of hysteresis overfitting and underfitting. Future work is required on the subject in order to develop several Preisach density function focused on compensating for a specific amount of Hysteresis Error. This task can be carried out for sensors exhibiting a linear output, such as the Tekscan A201-X, and for sensors with a nonlinear response, e.g. Interlink FSR40X and Peratech QTC sensors.

Acknowledgment

This study was supported by Colciencias through Francisco José de Caldas Fund (FP44842-335-2015) and by grant PI/UAN-2017-603GIBIO

References

[1] Overduin, S., Zaheer, F., Bizzi, E. and D'avella, A., An instrumented glove for small primates, Journal of Neuroscience Methods, 187(1), pp. 100-104, 2010. DOI: 10.1016/j.jneumeth.2009.12.007

[2] Fong, D. and Chan, Y.-Y., The use of wearable inertial motion sensors in human lower limb biomechanics studies: A systematic review, Sensors, 10(12), pp. 11556-11565, 2010. DOI: 10.3390/s101211556

[3] Fosty, B., Ben-Sadoun, G., Sacco, G., Konig, A., Manera, V., Foulon, P., Brisswalter, J., Robert, P.H. and Bremond., F., Accuracy and reliability of the rgb-d camera for measuring walking speed on a treadmill, Gait and Posture, 48, pp. 113-119, 2016. DOI: 10.1016/j.gaitpost.2016.04.011

[4] Faraz, M., Salcic, Z. and Wang, K., Analysis and selection of the force sensitive resistors for gait characterization, in Int. Conf. on Automation, Robotics and Applications, Feb 2015, pp. 370-375, Queenstown, New Zealand.

[5] Schofield, J., Evans, K., Hebert, J., Marasco, P. and Carey, J., The effect of biomechanical variables on force sensitive resistor error: Implications for calibration and improved accuracy, Journal of Biomechanics, 49(5), pp. 786-792, 2016. DOI: 10.1016/j.jbiomech.2016.01.022

[6] Tiwana, M., Redmond, S. and Lovell, N., A review of tactile sensing technologies with applications in biomedical engineering, Sensors and Actuators A: Physical, 179, pp. 17-31, 2012. DOI: 10.1016/j.sna.2012.02.051

[7] Interlink Electronics, FSR400 Series Datasheet, [online]. Available at: http://www.interlinkelectronics.com/datasheets/Datasheet_FSR.pdf.

[8] Tekscan Inc, FlexiForce, Standard Force & Load Sensors Model A201. Datasheet, [online]. Available at: https://www.tekscan.com /sites/default/files/resources/FLX-A201-A.pdf.

[9] Lebosse, C., Renaud, P., Bayle, B. and Mathelin, M., Modeling and evaluation of low-cost force sensors, IEEE Transactions on Robotics, 27(4), pp. 815-822, 2011. DOI: 10.1109/TRO.2011.2119850

[10] Hollinger, A. and Wanderley, M., Evaluation of commercial force-sensing resistors, in Int. Conf. on new interfaces for musical expression NIME06, 2006, Paris, France.

[11] Komi, E., Roberts, J., and Rothberg, S., Evaluation of thin, flexible sensors for time-resolved grip force measurement, Proc. Institution of Mechanical Engineers, Part C: Journal of Mechanical Engineering Science, 221(12), pp. 1687-1699, 2007. DOI: 10.1243/09544062JMES700

[12] Dabling, J., Filatov, A. and Wheeler, J., Static and cyclic performance evaluation of sensors for human interface pressure measurement, in Annual Int. Conf. of the IEEE Engineering in Medicine and Biology Society, Aug 2012, pp. 162-165, San Diego, CA.

[13] Vecchi, F., Freschi, C., Micera, S., Sabatini, A.M, Dario, P. and Sacchetti, R., Experimental evaluation of two commercial force sensors for applications in biomechanics and motor control, in Annual Conf. of the Int. Functional Electrical Stimulation Society, 2000, pp. 45-54, Aalborg, Denmark.

[14] Urban, S., Ludersdorfer, M. and Van der Smagt, P., Sensor calibration and hysteresis compensation with heteroscedastic gaussian processes, IEEE Sensors Journal, 15(11), pp. 6498-6506, 2015. DOI: 10.1109/JSEN.2015.2455814

[15] Paredes-Madrid, L., Torruella, P., Solaeche, P., Galiana, I. and Gonzalez-de Santos, P., Accurate modeling of low-cost piezoresistive force sensors for haptic interfaces, in Proc. IEEE Int. Conf. Robotics and Automation, 2010, pp. 1828-1833, Anchorage, AK. DOI: 10.1109/ROBOT.2010.5509436

[16] Paredes-Madrid, L., Emmi, L., Garcia, E. and Gonzalez-de Santos, P., Detailed study of amplitude nonlinearity in piezoresistive force sensors, Sensors, 11(9), pp. 8836-8854, 2011. DOI: 10.3390/s110908836

[17] Visone, C., Hysteresis modelling and compensation for smart sensors and actuators, Journal of Physics: Conference Series, 138(1), p. 012028, 2008. DOI: 10.1088/1742-6596/138/1/012028

[18] Stolt, A., Linderoth, M., Robertsson, A. and Johansson, R., Force controlled robotic assembly without a force sensor, in Proc. IEEE. Int. Conf. Robotics and Automation, May 2012, pp. 1538-1543, St. Paul, MN.

[19] Melnyk, A., Henaff, P., Khomenko, V. and Borysenko, V., Sensor network architecture to measure characteristics of a handshake

between humans, in Proc. IEEE Int. Conf. Electronics and Nanotechnology, April 2014, pp. 264-268, Kiev, Ukraine. DOI: 10.1109/ELNANO.2014.6873983
[20] Stakvik, J., Ragazzon, M., Eielsen, A. and Gravdahl, J., On implementation of the Preisach model identification and inversion for hysteresis compensation, Modeling, Identification and Control, 36(3), pp. 133-142, 2015. DOI: 10.4173/mic.2015.3.1
[21] Tan, X., Venkataraman, R. and Krishnaprasad, P., Control of hysteresis: Theory and experimental results, in SPIE's 8th Annual International Symposium on Smart Structures and Materials, 2001, pp. 101-112, Newport Beach, CA.
[22] Tan, X. and Bennani, O., Fast inverse compensation of Preisach-type hysteresis operators using field-programmable gate arrays, in 2008 American Control Conference, June 2008, pp. 2365-2370, Seattle, WA. DOI: 10.1109/ACC.2008.4586845

L. Paredes-Madrid, was born in Caracas, Venezuela in 1985. He received his BSc. degree in Electronic Engineering from Simon Bolivar University, Caracas, Venezuela, in 2007 and the PhD. degree in system engineering and automation from Complutense University of Madrid, Spain, in 2014. He has been a research assistant in the Centre for Automation and Robotics CSIC, Madrid, Spain and in Northwestern University, Evanston, IL. He is currently a full-time professor at Antonio Nariño University in Tunja, Colombia, since 2014. His research interests are the instrumentation and control of autonomous systems.
ORCID: 0000-0001-8609-0681

A. Matute, was born in Valencia, Venezuela in 1984. He received his BSc. and MSc. degree in 2008 and 2014 respectively, both in Electronic Engineering from Simon Bolivar University in Caracas, Venezuela. He has conducted research in the implementation of soft computing techniques for modelling of nonlinear systems and recently piezoresistive sensors. In addition, he worked at industry for eight years in managerial positions. Currently he continues research in piezoresistive sensors characterization at Antonio Nariño University in Tunja, Colombia.
ORCID: 0000-0002-6746-2168

A.F. Cruz-Pacheco, received his BSc. and MSc. degree in 2011 and 2015 respectively, both in Pedagogical and Technological University of Colombia –UPTC– in Tunja, Colombia. He has conducted research in Synthesis, characterization and evaluation of ceramics and materials in general. He is currently conducting research on characterization of piezoresistive materials in Pedagogical and technological University of Colombia.
ORCID: 0000-0003-3562-246X

C.A. Parra-Vargas, received his BSc. degree in physical and mathematics education from Pedagogical and Technological University of Colombia - UPTC, Tunja, Colombia, in 1990, In addition he is MSc. and Dr. in Physical Sciences from Universidad Nacional de Colombia, Bogotá, in 2005. He has conducted studies in research on characterization of materials in Pedagogical and Technological University of Colombia. He is currently a full-time professor at Pedagogical and technological University of Colombia in Tunja, Colombia.
ORCID: 0000-0001-8968-8654

E.I. Gutiérrez-Velásquez, received his BSc. degree in mechanical engineering and MSc. degree in engineering in 2001 and 2008 respectively, both from University of Antioquia in Medellín, Colombia and the PhD. degree in Mechanical Engineering from Federal University of Itajubá, Brazil, in 2013. He has conducted research in optimization and modelling of thermal systems. He is currently a full-time professor at Antonio Nariño University in Medellín, Colombia since 2014.
ORCID: 0000-0002-4326-946X